Article

Metastable CdSb: A Complex Structured Intermetallic Compound with Semiconductor Properties

Andreas Tengå, Sven Lidin, Jean-Philippe Belieres, N. Newman, Yang Wu, and Ulrich Häussermann

J. Am. Chem. Soc., **2008**, 130 (46), 15564-15572 • DOI: 10.1021/ja805454p • Publication Date (Web): 29 October 2008

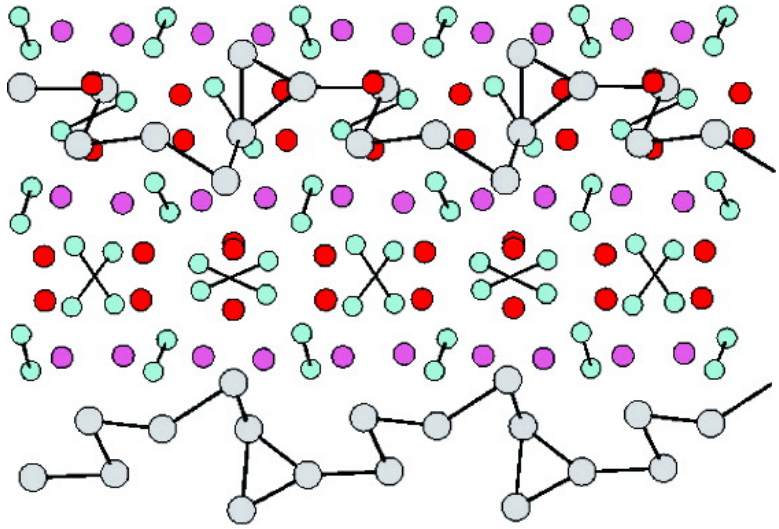

J|A|C|S
ARTICLES

Published on Web 10/29/2008

Metastable Cd_4Sb_3: A Complex Structured Intermetallic Compound with Semiconductor Properties

Andreas Tengå,[†] Sven Lidin,[†] Jean-Philippe Belieres,[‡] N. Newman,[§] Yang Wu,[‡] and Ulrich Häussermann*[,‡]

Inorganic Chemistry, Stockholm University, SE-10691 Stockholm, Sweden, Department of Chemistry and Biochemistry, Arizona State University, Tempe, Arizona 85287-1604, and School of Materials, Arizona State University, Tempe, Arizona 85287-8706

Received July 14, 2008; E-mail: Ulrich.Haussermann@asu.edu

Abstract: The metastable binary intermetallic compound Cd_4Sb_3 was obtained as polycrystalline ingot by quenching stoichiometric Cd−Sb melts and as mm-sized crystals by employing Bi or Sn fluxes. The compound crystallizes in the monoclinic space group *Pn* with $a = 11.4975(5)$ Å, $b = 26.126(1)$ Å, $c = 26.122(1)$ Å, $\beta = 100.77(1)°$, and $V = 7708.2(5)$ Å^3. The actual formula unit of Cd_4Sb_3 is $Cd_{13}Sb_{10}$ and the unit cell contains 156 Cd and 120 Sb atoms ($Z = 12$). Cd_4Sb_3 displays a reversible order−disorder transition at 373 K and decomposes exothermically into a mixture of elemental Cd and CdSb at around 520 K. Disordered β-Cd_4Sb_3 is rhombohedral (space group $R\bar{3}c$, $a \approx 13.04$ Å, $c \approx 13.03$ Å) with a framework isostructural to β-Zn_4Sb_3. The structure of monoclinic α-Cd_4Sb_3 bears resemblance to the low-temperature modifications of Zn_4Sb_3, α- and α'-Zn_4Sb_3, in that randomly distributed vacancies and interstitial atoms of the high-temperature modification aggregate and order into distinct arrays. However, the nature of aggregation and distribution of aggregates is different in the two systems. Cd_4Sb_3 displays the properties of a narrow gap semiconductor. Between 10 and 350 K the resistivity of melt-quenched samples first increases with increasing temperature until a maximum value at 250 K and then decreases again. The resistivity maximum is accompanied with a discontinuity in the thermopower, which is positive and increasing from 10 to 350 K. The room temperature values of the resistivity and thermopower are about 25 mΩcm and 160 μV/K, respectively. Flux synthesized samples show altered properties due to the incorporation of small amounts of Bi or Sn (less than 1 at. %). Thermopower and resistivity appear drastically increased for Sn doped samples. Characteristic for Cd_4Sb_3 samples is their low thermal conductivity, which drops below 1 W/mK above 130 K and attains values around 0.75 W/mK at room temperature, which is comparable to vitreous materials.

Introduction

Intermetallic compounds are capable of unrivaled structural complexity in the atomic arrangement of their crystalline phases. This is already (or perhaps especially) apparent in binary systems and prominent examples are classic "giant unit cell crystals" like $NaCd_2$ or Mg_2Al_3,[1−4] γ-brass derivatives like Rh_7Mg_{44} or $Ir_{11}Zn_{91}$[5] and quasicrystal approximants occurring in numerous alkaline-earth and rare-earth Zn and Cd systems.[6] These phases all have structures with several hundred up to 1200 atoms in unit cells with edges several nm long. Binary intermetallic systems even afford stable icosahedral quasicrystals.[7]

Lately it has been suggested that complex structured intermetallics may display interesting transport properties arising from the different length scales of cluster building blocks and lattice periodicity, or from the frequently occurring disorder in the form of mixed and fractional site occupancies.[4,8] For instance, complex structured materials are prone to have low thermal lattice conductivities because the probability of Umklapp processes that scatter heat carrying phonon scales with the unit cell size, and/or the presence of disorder facilitates defect scattering.[9,10] Quasicrystals and approximants typically exhibit thermal lattice conductivity values on the order of 1−3 W/mK, which compares to ceramics and glasses and has made them attractive for use as thermal barrier coatings.[11] Further, if structural complexity can be combined with a narrow band gap,

[†] Stockholm University.
[‡] Department of Chemistry and Biochemistry, Arizona State University.
[§] School of Materials, Arizona State University.

(1) Samson, S. *Nature* **1962**, *195*, 259.
(2) Samson, S. *Acta Crystallogr.* **1965**, *19*, 401.
(3) Fredrickson, D. C.; Lee, S.; Hoffmann, R. *Angew. Chem., Int. Ed.* **2007**, *46*, 1958.
(4) Feuerbacher, M.; et al. *Z. Kristallogr.* **2007**, *222*, 259.
(5) Berger, R. F.; Lee, S.; Johnson, J.; Nebgen, B.; Sha, F.; Xu, J. Q. *Chem.−Eur. J.* **2008**, *14*, 3908.
(6) Villars, P.; Calvert, L. D. *Pearsons Handbook of Crystallographic Data for Intermetallic Compounds*, 2nd ed.; ASM International: Materials Park, OH, 1991; Desk Edition, 1997.
(7) Tsai, A. P.; Gou, J. Q.; Abe, E.; Takakura, H.; Sato, T. J. *Nature* **2000**, *408*, 537.
(8) Urban, K.; Feuerbacher, M. *J. Non-Cryst. Solids* **2004**, *334&335*, 143.
(9) Slack, G. A. In *Solid State Physics*, Vol. 34; Ehrenreich, H.; Seitz, F.; Turnbull D., Eds.; Academic Press: New York, 1979; pp 1−71.
(10) Tritt, T. M., Ed. *Thermal Conductivity: Theory, Properties and Applications*; Springer: New York, 2004.
(11) Pope, A. L.; Tritt, T. M. In *Thermal Conductivity: Theory, Properties and Applications*; Tritt, T. M., Ed.; Springer: New York, 2004; pp 255−259.

10.1021/ja805454p CCC: $40.75

possibilities arise for promising thermoelectric properties. Reasonably high Seebeck coefficients S and electric conductivities σ inherent to narrow band gap semiconductors may then be combinable with a low thermal conductivity κ, which—according to the thermoelectric figure of merit $z = S^2\sigma/\kappa$—yields an efficient material.[12,13] The total thermal conductivity κ is a sum of an electronic and the lattice contribution, κ_e and κ_L, respectively, where κ_e is proportional to the electric conductivity.

Zn_4Sb_3 is a binary intermetallic in which semiconductor electron transport properties seem to be compatible with an extraordinarily low thermal conductivity. Originally, a room temperature value of 0.9 W/mK was reported for κ, and the lattice contribution was estimated to 0.65 W/mK, which is lower than for quasicrystals.[14] Consequently much work has been devoted to understanding the possible origin of this low thermal conductivity. The discovery that the room temperature form of Zn_4Sb_3, β-Zn_4Sb_3, is intricately disordered and exhibits vacancies and interstitial Zn atoms provided an important step.[15,16] However, recent inelastic neutron scattering measurements indicate that instead of occupational disorder rather dynamical disorder from a peculiar feature of the regular structure - Sb_2 dumbbells - may be the origin of the "phonon glass" behavior.[17] The debate suggests that phonon scattering mechanisms in Zn_4Sb_3 are complicated and underlines the general difficulty in establishing fundamental crystal structure/property correlations in complex structured materials. As a further peculiarity, β-Zn_4Sb_3 undergoes a sequence of low-temperature transitions into highly complex structures where vacancies and interstitials are ordered into distinct islands.[18−20] These ordering processes allowed the determination of the actual composition of Zn_4Sb_3 ($Zn_{13-\delta}Sb_{10}$) and can be regarded as intrinsic Zn nanocrystal formation within the rhombohedral, high symmetry Zn−Sb framework of the room temperature phase. Interestingly, low-temperature ordering seems to have only a minor consequence to the thermal conductivity of Zn_4Sb_3.[19,21]

The peculiarities of Zn_4Sb_3 raise the question if there are more binary intermetallic compounds that combine semiconductor properties with a low thermal conductivity. Here we report on the structure and property characterization of Cd_4Sb_3. It appears self-evident to look at the heavier analogue, however, in contrast to Zn_4Sb_3, Cd_4Sb_3 is metastable[22] and reports of its thermodynamic, structural and physical properties are contradictory.[23] Samples of Cd_4Sb_3 can be obtained from the solidification of undercooled melts and powder diffraction patterns resemble that of β-Zn_4Sb_3. A recent single crystal X-ray structure investigation of Cd_4Sb_3 seemed to confirm that β-Zn_4Sb_3 and Cd_4Sb_3 are isostructural.[24] Our study, however, reveals that Cd_4Sb_3 possesses an ordered and complex room temperature structure with a crystallographic composition $Cd_{13}Sb_{10}$. This structure is similar to that of low temperature α-Zn_4Sb_3. The electron transport properties of Cd_4Sb_3 differ from Zn_4Sb_3, while the thermal lattice conductivity is comparably low.

2. Experimental Section

Synthesis and Phase Characterization. Starting materials were granules of Cd (99.9%, 5−20 mesh), powder of Sb (99.5%, ~100 mesh), shots of Sn (99.999%), and pieces of Bi (99.999%, 1−12 mm) purchased from Sigma-Aldrich. Prior heat treatment reaction mixtures were pressed into pellets. Polycrystalline ingots of Cd_4Sb_3 were prepared by placing a mixture (1−3 g batches) with the composition $Cd_{57}Sb_{43}$ (Cd_4Sb_3) within evacuated fused silica tubes. The tubes were heated to 923 K, kept at this temperature for 24 h and occasionally shaken to ensure complete melting and mixing of all metals, and subsequently quenched to room temperature.

Large, mm-sized, crystals of Cd_4Sb_3 were synthesized from mixtures (3−5 g batches) with the composition $Cd_{50}Sb_{25}Bi_{25}$ and $Cd_{50}Sb_{25}Sn_{25}$ which were loaded into a specially prepared evacuated fused silica tube. The tube was placed in a well insulated stainless steel container. For details see ref 25. The container was heated to 923 K, kept at this temperature for 24 h and occasionally shaken. Thereafter, the temperature was lowered at a rate of 50 K/h to a temperature 20 K above the crystallization temperature of Cd_4Sb_3 in the prevailing metal flux. (This temperature was determined prior from differential thermal analysis (DTA) runs where 0.1 g of the starting composition was loaded and sealed in a stainless steel pan in an argon atmosphere, heated under a flow of Ar to 923 K, and cooled to room temperature at a rate of 5 K/min.) After approaching the crystallization temperature of ~600 K, the cooling rate was lowered to 1 K/h and the melt cooled at this rate until a temperature of 523 K was reached. At this temperature the product was separated from the liquid excess metal mixture by centrifugation.

Powder X-ray diffraction patterns collected either on a Guiner camera (Cu Kα_1 radiation) or a Siemens D5000 diffractometer (Cu Kα radiation) were identical for melt-quenched prepared and flux synthesized Cd_4Sb_3 and indicated the rhombohedral structure ($R\bar{3}c$, $a \approx 13.04$ Å, $c \approx 13.03$ Å) suggested earlier by Zelinska et al.[24] The composition of the products was analyzed by electron microprobe analysis (EPMA) in a JEOL JXA-8600 microscope operated at 15.0 kV and 30.0 nA. Samples were enclosed in epoxy and polished. Elemental metals were used as standards for Sb, Zn, and Sn, while Bi_2S_3 was used for Bi. The ZAF correction procedure was employed for quantitative composition determination.

Thermal Analysis. Five to 20 mg of sample was hermetically sealed under Argon atmosphere in a TA Tzero aluminum pan. Differential Scanning Calorimetry (DSC) was performed using a "heat flux" calorimeter TA Instrument 2910 under a Helium gas flow of ~30 mL/min. Scanning ranges were from 323 to 393 K and from 323 to 723 K with a heating/cooling rate of 5 K/min. At the maximum temperature the sample was equilibrated for 5 min. A baseline calibration was performed to compensate for the cell heat flow imbalance between reference and sample positions. Temperature and heat flow were calibrated using Indium (T_m= 429.8 K, ΔH_{fus}= 28.58 J/g) and Zinc (T_m= 692.7 K). DCS curves and enthalpy of transitions were accessed with the TA Instruments software, Universal Analysis 2000.

Crystal Structure Characterization. Crystals for single crystal X-ray diffraction were obtained by crushing parts of flux-synthesized and melt-quenched specimens. Initial examinations showed that Cd_4Sb_3 crystals generally were pseudomerohedrally twinned, exhibiting the trigonal Laue symmetry $\bar{3}m$. In this respect there

(12) Mahan, G. D. *J. Appl. Phys.* **1989**, *65*, 1578.
(13) DiSalvo, F. J. *Science* **1999**, *285*, 703.
(14) Caillat, T.; Fleurial, J.-P.; Borshchevsky, A. *J. Phys. Chem. Solids* **1997**, *58*, 1119.
(15) Snyder, G. J.; Christensen, M.; Nishibori, E.; Caillat, T.; Iversen, B. B. *Nat. Mater.* **2004**, *3*, 458.
(16) Cargnoni, F.; Nishibori, E.; Rabiller, P.; Bertini, L.; Snyder, G. J.; Christensen, M.; Gatti, C.; Iversen, B. B. *Chem.−Eur. J.* **2004**, *10*, 3862.
(17) Schweika, W.; Hermann, R. P.; Prager, M.; Persson, J.; Keppens, V. *Phys. Rev. Lett.* **2007**, *99*, 125501.
(18) Nylén, J.; Andersson, M.; Lidin, S.; Häussermann, U. *J. Am. Chem. Soc.* **2004**, *126*, 16306.
(19) Nylén, J.; Lidin, S.; Andersson, M.; Iversen, B. B.; Liu, H. X.; Newman, N.; Häussermann, U. *Chem. Mater.* **2007**, *19*, 834.
(20) Nylén, J.; Lidin, S.; Andersson, M.; Liu, H.; Newman, N.; Häussermann, U. *J. Solid State Chem.* **2007**, *180*, 2603.
(21) Bhattacharya, S.; Hermann, R. P.; Keppens, V.; Tritt, T. M.; Snyder, G. J. *Phys. Rev. B* **2006**, *74*, 134108.
(22) Kirii, V. G.; Kirii, A. V.; Nikishina, I. V.; Marenkin, S. F. *Inorg. Mater.* **1997**, *33*, 654.
(23) Ugai, Y. A.; Averbakh, E. M.; Marshakova, T. A.; Matveev, O. V. *Sov. Phys.−Solid State* **1962**, *4*, 448.
(24) Zelinska, O. Y.; Bie, H. Y.; Mar, A. *Chem. Mater.* **2007**, *19*, 1518.

Table 1. Summary of Crystallographic Data and Structural Analysis for α-Cd_4Sb_3

	α-Cd_4Sb_3 (room temperature)	α-Cd_4Sb_3 (low temperature)
formula	$Cd_{13}Sb_{10}$	$Cd_{13}Sb_{10}$
formula weight	1734.43	1734.43
crystal habit	irregular	irregular
crystal size, mm^3	0.02*0.08*0.10	0.02*0.08*0.10
space group	*P1n1* (No. 7)	*P1n1* (No. 7)
a, Å	11.4975(5)	11.4478(4)
b, Å	26.1262(10)	26.0793(7)
c, Å	26.1281(10)	26.0691(10)
β, deg	100.777(4)	100.872(4)
Z; *V*, $Å^3$	12;7708(5)	12;7643(1)
*D*calc, gcm^{-3}	6.984	7.128
temp, K	293(2)	100(2)
λ(Mo Kα), Å	0.71069	0.71069
absorption coeff, mm^{-1}	21.06	21.06
F(000)	13342	13608
θmin-θmax, deg	3.66−31.95	3.65−31.94
index ranges	$-13 < h < 16$, $-35 < k < 38$, $-22 < l < 37$	$-13 < h < 16$, $-35 < k < 38$, $-22 < l < 37$
total reflns collected	28569	28443
independent reflns	5408 [*R*(int) = 0.0570]	7624 [*R*(int) = 0.0611]
refinement method	full-matrix least-squares on F^2	full-matrix least-squares on F^2
data/restraints/params	5408/0/419	7624/0/419
final *R* indices [$I > 3\sigma(I)$][a,b]	*R*1 = 0.0606, *wR*2 = 0.1410	*R*1 = 0.0607, *wR*2 = 0.1367
R indices (all data)[a,b]	*R*1 = 0.2112, *wR*2 = 0.1856	*R*1 = 0.1734, *wR*2 = 0.1773
largest diff. peak and hole, êA^{-3}	7.24 and −5.91	11.81 and −7.17
GOF on F^2	1.12	1.21

[a] $R_1) \Sigma||Fo| - |F||/\Sigma|F_o|$. [b] $wR_2 = \{\Sigma[w(Fo^2 - Fc^2)^2]/\Sigma[w(Fo^2)^2]\}^{1/2}$.

was no difference between flux-synthesized and melt-quenched sample. A crystal from the melt-quenched sample was then selected for a complete intensity data collection which was performed at room temperature (295 K) and 100 K on an Oxford Diffraction Xcalibur 3 CCD diffractometer with monochromatic Mo Kα radiation (λ = 0.71073 Å) operated at 50 kV and 40 mA and equipped with an Oxford cryo system cooler. The sample-to-detector distance was 50 mm. Oxford Diffraction's CrysAlis software was employed for data reduction.[26] Structure refinements were performed by using the program package JANA2000.[27]

The X-ray diffraction pattern reveals a subset of strong reflections indexable by the hexagonal cell, $a \approx 13.04$ Å, $c \approx 13.03$ Å) of the rhombohedral structure reported by Zelinska et al.[24] Additionally, a weaker set of reflections appear to yield a very large supercell, but systematic, noncrystallographic absences among them suggests twinning. Considering pseudomerohedral twinning, all reflections are indexable by a monoclinic cell a = 11.4975(5) Å, b = 26.1262(10) Å, c = 26.1218(11) Å, β = 100.776(4)°. This cell was used for the evaluation of the data. The relation between the hexagonal and the monoclinic cell are given by the matrix M = [(2/3, 1/3, −2/3) (0, −2, 0) (−2, −1, −1)]. The maximal symmetry of this cell from systematic absences and group-subgroup relations is $P2_1/n$.

Due to the twinning, and the severe pseudosymmetry of the data, straightforward solution by standard methods was not possible. Instead, direct methods were used to generate a seed solution in the monoclinic unit cell with the approximate composition $Cd_{15}Sb_{10}$. Assignment of Cd/Sb was based on the rhombohedral structure. In this seed structure, a number of interstitial Cd positions could be identified, and for these, occupancies were refined. For all Cd positions a common isotropic displacement parameter was used, and the same procedure was used for Sb. The seed structure was now refined (on F), and the solution was regularly inspected. Cd positions that had close contacts to other Cd positions were converted to interstitials, interstitial positions with low occupancy parameters were removed, and in positions with high positive residual electron densities, new interstitial positions were inserted with low, refinable, occupancies. This refinement was repeated over many cycles, until a solution with no low occupancies and no short distances was identified.

This procedure was performed in the space groups $P2_1/n$, Pn, $P2_1$, and $P\bar{1}$ but convergence was achieved only in Pn. The final model contained 64 Cd positions corresponding to the 36f Cd site in the rhombohedral structure (space group $R\bar{3}c$) and 14 Cd positions corresponding to interstitial sites. Also the 60 Sb positions were grouped in two sets corresponding to the 12c and 18e positions in the rhombohedral structure, respectively. Atom sites within each group were given the same isotropic displacement parameter and the model was refined against F^2.

The refinement was carried out for the two data sets (295 and 100 K). In both cases, the twinning was modeled using three twin components, and as the relative size of the two minor subvolumes was subject to large fluctuations, their ratio was fixed to unity. Both refinements resulted in a twin ratio very close to 0.5 for the main subvolume. The internal consistency (R_{int}) for the two data sets was between 4 and 5%. The final model contains 418 parameters (138 atomic positions yielding 412 positional parameters, 4 isotropic displacement parameters and 2 scale factors). The difference between the two refinements lies mainly in the displacement parameters. In particular those of the interstitial Cd atoms are very much reduced in the low temperature refinement. The largest residuals (12e/$Å^3$) in the electron density map correspond to a position at, or close to the Cd3 site, but any attempt to introduce new positions at these maxima results in occupancies that approach zero, or positions that coalesce with the Cd3 positions. Table 1 lists a summary of the refinement results. Details are supplied as Supporting Information.

Physical Property Measurements. The electrical resistivity, thermopower and thermal conductivity of Cd_4Sb_3 were measured on a Physical Property Measurement System (PPMS) from Quantum Design equipped with the Thermal Transport Option (TTO). Brick-like crystals from flux synthesized Cd_4Sb_3 and a piece from a fragmented ingot of melt-quenched Cd_4Sb_3 were selected and polished into blocks with dimensions 1.55 × 1.55 × 2.95 mm (melt-

(25) Boström, M.; Hovmoller, S. *J. Solid State Chem.* **2000**, *153*, 398.
(26) *CrysAlis*, Software for automated data collection and reduction, Oxford Diffraction, 2006.
(27) Petricek, V.; Dusek, M. *The crystallographic computing system JANA2000*, Institute of Physics, Praha, Czech Republic, 2000.

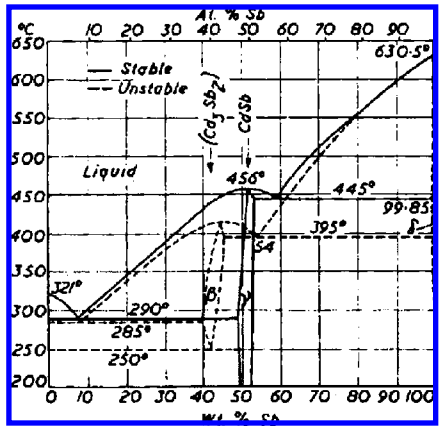

Figure 1. Phase diagram of the binary Cd−Sb system according to ref 30 (also see ref 31).

quenched sample), 1.35 × 2.25 × 2.50 mm (Bi-flux sample) and 1.95 × 1.60 × 1.85 mm (Sn-flux sample). Two copper disks with extruded leads on each end were glued oppositely onto the specimen using a two-component silver-filled epoxy (Epo-Tek H20E), which provided contact after curing at slightly elevated temperatures for a short time. The arrangement was then mounted on the TTO puck, which was subsequently loaded into the PPMS chamber and then evacuated to high vacuum ($<10^{-3}$ torr) for the measurement. The thermal transport measurements were conducted in a two-point configuration from 10 to 350 K at a scanning rate of 0.3 K/min. At a certain temperature, a heat pulse was applied to the sample to create a temperature gradient. Thermal conductivity and Seebeck coefficient were obtained when the sample was equilibrated. Resistivity was then acquired by introducing up to a maximum value of 1.5 mA AC current at a frequency of 17 Hz. The autorange feature was used in all of the measurements in the PPMS system. Radiation heat loss was automatically corrected automatically with the incorporated functions of the software.

3. Results and Discussion

Synthesis and Phase Analysis of Cd4Sb3. In contrast to the Zn−Sb system, which affords three fields of phases (ZnSb, Zn_4Sb_3, and Zn_3Sb_2), the Cd−Sb system contains only equiatomic CdSb as a stable phase (Figure 1).[28] CdSb is isostructural to ZnSb.[29] In addition, a metastable phase field between 523 and 693 K embracing the compositions Cd_3Sb_2 and Cd_4Sb_3 has been suggested.[30] Equilibria between stable and metastable phases make the Cd−Sb system quite complex.[31] The crystallization behavior of the metastable phases Cd_3Sb_2 and Cd_4Sb_3 is obscure and depends on the degree of superheat, which suggests that metastable equilibria are also present in the melt.[32] Although a substantial amount of work has been devoted to the Cd−Sb system, especially by Russian researchers,[28−32] it is far from completely understood.

Melts with a composition Cd:Sb ≈ 4:3 can be easily undercooled and single phase Cd_4Sb_3 solidifies as a polycrystalline ingot over a wide range of cooling rates.[22] Figure 2 shows the DSC heating and cooling cycle of a melt-quenched Cd_4Sb_3 sample. Upon heating a sharp endothermic event occurs at 373

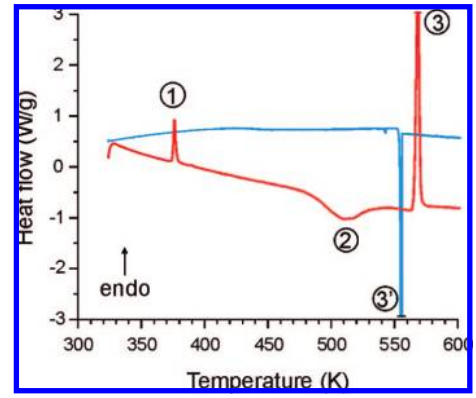

Figure 2. DSC heating (red line) and cooling trace (blue line) of Cd_4Sb_3. The thermal events are: (1) structural phase transition, (2) decomposition into Cd+CdSb, (3) melting of mixture Cd+CdSb, (3′) recrystallization of Cd+CdSb.

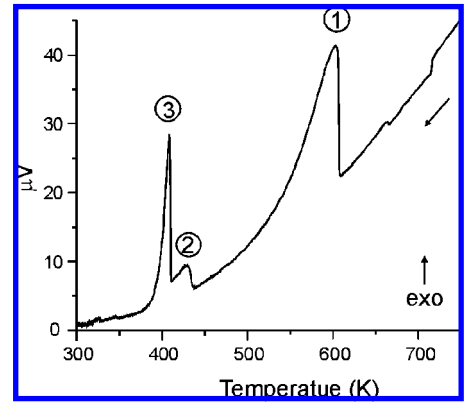

Figure 3. DTA cooling trace for $Cd_{50}Sb_{25}Bi_{25}$. The thermal events are: (1) Crystallization of Cd_4Sb_3, (2) crystallization of Bi, (3) crystallization of eutectic mixture Cd−Bi.

K, which corresponds - as we will show later - to a reversible structural phase transition. This is in accordance with Kirii et al. who reported DTA traces of differently quenched melts that all showed a thermal event at around 377 K.[22] The broad exothermic event with a maximum around 525 K corresponds to the decomposition of metastable Cd_4Sb_3 into a mixture of Cd and CdSb. It has been reported that the decomposition temperature may vary between 491 and 693 K depending on the thermal history of the material and probably the heating rate applied.[22] Stable eutectic Cd + CdSb then melts at 563 K (290 °C, cf Figure 1). Upon cooling from 723 K eutectic Cd + CdSb recrystallizes at 557 K and no further event is observed at lower temperature. Powder X-ray diffraction confirms that the solidified sample constitutes of a mixture of Cd and CdSb.

The crystallization behavior of Cd_4Sb_3 and the phase relations in the Cd−Sb system are drastically changed in the presence of Bi. The Cd−Bi phase diagram is of the simple eutectic type with almost zero mutual solubility of the elements in the solid.[28] The Sb−Bi system displays continuous miscibility in the solid and liquid.[28] Figure 3 shows the DTA cooling trace of a mixture $Cd_{50}Sb_{25}Bi_{25}$ that has been heated to 923 K. Upon cooling this mixture Cd_4Sb_3 crystallizes at 608 K, which consumes virtually all of the Sb and leaves a melt with an approximate composition $Cd_{17}Bi_{25}$ ($Cd_{40}Bi_{60}$). The next event is the crystallization of pure Bi from this melt at a temperature according to its composition. The third event is the crystallization of the eutectic mixture ($\sim Cd_{55}Bi_{45}$) at 419 K.[28] A similar DTA cooling trace is obtained

(28) Massalski, T. S. *Binary Alloy Phase Diagrams*, 2nd ed.; American Society for Metals: Metals Park, OH, 1990.
(29) Range, K.-J.; Pfauntsch, J.; Klement, U. *Acta Crystallogr. C* **1988**, *44*, 2196.
(30) Gale, W. F.; Totemeier, T. C., Eds. *Smithells Metals Reference Book*, 8th ed.; Elsevier Butterworth-Heinemann: Oxford, UK, 2004.
(31) Psarev, V. I.; Kostur, T. A. *Inorg. Mater.* **1977**, *13*, 1708.
(32) Pavlova, L. M.; Dolgopolava, E. A. *Inorg. Mater.* **1987**, *23*, 166.

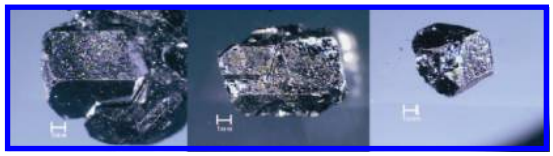

Figure 4. Photographs of Cd_4Sb_3 crystals obtained from a Bi flux (left and middle) and from a Sn flux (right).

Table 2. Electron Microprobe Determined Compositions of Differently Prepared Samples of Cd_4Sb_3 (X = Bi, Sn)

	melt-quenched	Bi-flux	Sn-flux
Cd	56.76 ± 0.22	56.44 ± 0.70	57.43 ± 0.26
Sb	43.23 ± 0.19	42.79 ± 0.75	42.48 ± 0.28
X	−	0.91 ± 0.40	0.092 ± 0.037

for $Cd_{50}Bi_{25}Sn_{25}$. The presence of Bi or Sn (X) does not afford a ternary compound Cd−Sb−X, although small amounts of X are incorporated in Cd_4Sb_3. Instead, the crystallization of Cd_4Sb_3 is facilitated and the formation of the other metastable Cd−Sb phase, Cd_3Sb_2, suppressed. With this finding, crystals of Cd_4Sb_3 are easily grown by slowly cooling ternary melts. Although no particular effort was undertaken to find optimum growth conditions, crystal specimens with sizes up to 5 × 5 × 7 mm were obtained (Figure 4).

In flux synthesized Cd_4Sb_3 additional metal atoms are unavoidably incorporated in small concentrations. Table 2 compares the composition of melt-quenched and fluxed synthesized samples as obtained from microprobe analysis. The average composition of the melt-quenched sample is close to Cd_4Sb_3 ($Cd_{57}Sb_{43}$). The analysis of the Bi-flux sample suggests that Bi replaces Sb (0.9 at.%), whereas the one for the Sn-flux prepared sample is not conclusive. Only a very small amount of Sn (0.1 at.%) was found to be incorporated, however, at the same time the Cd content appears increased. As it is shown later, the crystallographic composition of Cd_4Sb_3 is $Cd_{13}Sb_{10}$ (corresponding to 56.5 at.% Cd) and it is not clear if Sn-flux conditions create Sb vacancies or Cd/Sb mixed occupancy in Cd_4Sb_3. Also, we cannot exclude the possibility of Cd enrichment at the surface of Sn-flux crystals or general problems associated with the EPMA measurements.

The incorporation of a third metal has consequences to thermal (and electronic) properties of Cd_4Sb_3. This holds especially true for the Sn-flux prepared sample. Figure 5 shows DSC heating and cooling cycles for the differently prepared samples performed between 320 and 400 K. All samples display a reversible thermal event in this temperature range. This event is at 373 K for the melt-quenched sample, but shifted to lower temperatures (by about 20 K) for the flux synthesized samples. Additionally, the Sn-flux sample displays a large hysteresis, which however reproduces exactly upon cycling. The enthalpy values associated with this event are between 1 and 1.5 J/g.

Powder X-ray patterns of melt-quenched and flux prepared Cd_4Sb_3 resemble that of rhombohedral, disordered, β-Zn_4Sb_3. The β-Zn_4Sb_3 structure has been suggested for Cd_4Sb_3 earlier by Ugai et al.[33] and more recently by Zelinska et al.[24] Indeed, diffraction lines can be indexed with a hexagonal cell although the practically identical size of the *a* and *c* lattice parameter (≈13.03 Å) cause an increased number of accidental overlap. However β-Zn_4Sb_3 undergoes a low temperature structural

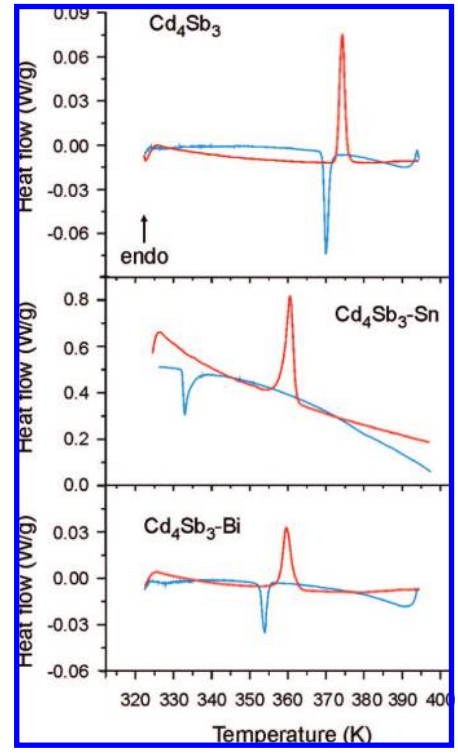

Figure 5. DSC heating (red lines) and cooling traces (blue lines) across the order−disorder α−β transition for melt-quenched (top), Sn-flux (middle), and Bi-flux (bottom) prepared samples of Cd_4Sb_3. The traces from a repeating cycle (not shown) are virtually identical.

transition into ordered α-Zn_4Sb_3. The reversible thermal event around 373 K raises the suspicion that a similar phenomenon occurs for Cd_4Sb_3 and that its room temperature form actually corresponds to an ordered α-phase. Careful inspection of the powder patterns did not reveal additional reflections or splitting of diffraction lines indicative of a superstructure.[34] Single crystal X-ray diffraction, however, showed readily the presence of a complex, monoclinic, superstructure for Cd_4Sb_3 at room temperature and below (100 K). Data collection at 423 K yielded then the rhombohedral structure which agreed with the model of Zelinska et al.[24] This shows unambiguously that the thermal event at 373 K corresponds to a reversible order−disorder structural transition. The reason for the discrepancy between ref 24 and our result is not clear. Since the superstructure is prominently evident in single crystal diffraction data, we do not believe that it could have been overlooked by Zelinska et al. using a state-of-the-art CCD diffractometer. Therefore it might be possible that metastable Cd_4Sb_3 is obtainable in the disordered β-modification at room temperature.

Crystal Structure of α-Cd4Sb3. Cd_4Sb_3 displays a reversible order(α)−disorder(β) transition. This phenomenon is also observed for Zn_4Sb_3, although the transition temperature for the latter is considerably lower (254 K instead of 373 K). The structure of α-Cd_4Sb_3 bears resemblance to α-Zn_4Sb_3, but is more complex. To establish structural relationships it is useful to recapitulate the main features of the rhombohedral β-Zn_4Sb_3 structure (space group $R\bar{3}$m). The crystal structure of hypotheti-

(33) Ignatev, N. A.; Ugai, Y. A.; Aleiniko, K. B.; Rabotkin, N. S. *Zh. Strukturnoi Khim.* **1971**, *12*, 729.

(34) In-house powder diffraction may not be able to discern α-Cd_4Sb_3 from β-Cd_4Sb_3. There are very few peaks of the α-phase that do not overlap with the β-phase. Most distinct should be the low angle reflections 021 and 120, which however did not reveal even after long exposure times.

cal disorder-free β-Zn_4Sb_3 (i.e., a framework $Zn_{12}Sb_{10}$) consists of three distinct atomic positions (36f Zn, 18e Sb1, 12c Sb2).[35] Zn and Sb1 display a peculiar 5- and 6-coordination, respectively, and form planar rhomboid rings, Zn_2Sb1_2—with a short Zn contact (2.8 Å)—that are further condensed into chains by sharing common Sb1 atoms (Figure 6a). These chains run in three different directions and are linked by Zn−Sb1 bonds, which results in channels along the c direction (Figure 6b). In the final framework $Zn_{12}Sb_{10}$ the channels are centered by Sb2 atoms, which attain a tetrahedral 4-coordination by binding to an additional Sb2 atom and to three Zn atoms residing in rhomboid ring chains. Zn disorder in β-Zn_4Sb_3 manifests in interstitial Zn atoms distributed on three weakly occupied (to about 6%) general sites 36f. Additionally, the regular Zn position displays a considerable occupational deficiency (89−90%).[15,16]

In ordered α-Cd_4Sb_3 and α-Zn_4Sb_3 framework and interstitial divalent atoms are located on distinct crystallographic sites. The ideal crystallographic composition of both phases is $Cd(Zn)_{13}Sb_{10}$. For Cd_4Sb_3 (melt-quenched sample) this composition (56.5 at.% Cd) is close to the one established by microprobe analysis (cf. Table 2), while Zn_4Sb_3 is known to be Zn deficient ($Zn_{13-\delta}Sb_{10}$)[15,16,18−20] and melt-quenched samples usually have a Zn concentration around 55.5 at. %.[20] The α-form of Cd_4Sb_3 crystallizes in the monoclinic space group *Pn* with a = 11.4975(5) Å, b = 26.126(1) Å, c = 26.122(1) Å, β = 100.77(1)°, and V = 7708.2(5) Å^3. The unit cell contains 156 Cd and 120 Sb atoms (Z = 12). The α-Zn_4Sb_3 structure is triclinic (space group $P\bar{1}$) with a metrically monoclinic unit cell ($a \approx$ 32.51 Å, $b \approx$ 12.23 Å, $c \approx$ 10.87 Å, $\beta \approx$ 99 °, $V \approx$ 4267 Å^3) which contains 104 Zn and 80 Sb atoms (Z = 8).[18]

Figure 6c and d depict sections of the α-Zn_4Sb_3 and α-Cd_4Sb_3 structure, respectively, projected along the direction equivalent to the hexagonal [001] direction in the rhombohedral β-Zn_4Sb_3 structure (cf. Figure 6b). These projections convey an impression of the deviation of the low-symmetry structures from rhombohedral $\bar{3}$ symmetry. It is easily noticeable that Sb atoms and pairs of Zn(Cd) atoms being part of rhomboid rings deviate only weakly. The symmetry reduction is largely caused by the arrangement of ordered interstitial Zn(Cd) atoms which are not part of the rhomboid ring framework.

For detailed comparison it is now convenient to describe the rhombohedral β-Zn_4Sb_3/β-Cd_4Sb_3 structure with a C-centered monoclinic unit cell (space group *C*2/*c*) with $a(c)$ = 10.88/11.47 Å, b = 12.225/13.004 Å, $c(a)$ = 8.18/8.68 Å, and $\beta \approx$ 100°. The monoclinic a and c axes may be interchanged and the monoclinic b axis coincides with the hexagonal a (or b) axis. The monoclinic cell is 2/3 of the size of the regular hexagonal unit cell and the relationships between monoclinic, rhombohedral and hexagonal axes have been worked out in detail by Mozharivskyj et al.[36] Figure 7a shows the framework of the β-structure projected on the monoclinic (bc) plane. This perspective reveals lamellae A repeating along the c direction and the repeat unit corresponds to two of such lamellae. In the α-Zn_4Sb_3 structure (Figure 7b) quadrupling in the stacking direction (long axis a) takes place and the repeat unit consists of 8 lamellae. Three consecutive lamellae contain interstitial Zn atoms (and are grouped to a block B), while the forth one is devoid of these. Finally in the α-Cd_4Sb_3 structure (Figure 7c) interstitials are contained in two consecutive lamellae (giving a shorter block B) which are separated by an interstitial free one. With respect to the β-structure (cf. Figure 7a) this leads to a trebling in the stacking direction (long axis c). Additionally, the translational period in the b direction, which is the same for β- and α-Zn_4Sb_3, is doubled for α-Cd_4Sb_3. Using the monoclinic system as a reference, the unit cells of α-Zn_4Sb_3

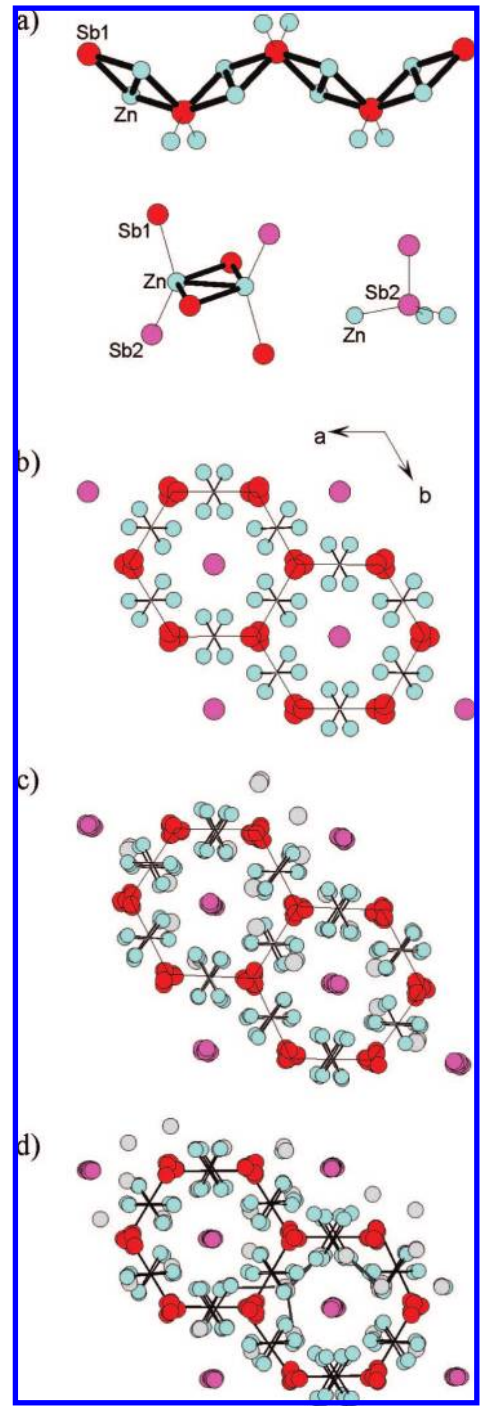

Figure 6. (a) Building units of the rhombohedral $Zn_{12}Sb_{10}$ framework of hypothetical, disorder-free β-Zn_4Sb_3. Turquoise circles denote Zn atoms, red and purple circles denote the two different types of Sb atoms (Sb1 and Sb2, respectively). Rhomboid rings Zn_2Sb1_2 (emphasized with bold lines) are condensed into chains (top). Coordination environment for Zn (bottom left) and Sb2 (bottom right). (b) The framework $Zn_{12}Sb_{10}$ projected along [001]. It contains channels which are stuffed by Sb2 atoms. For clarity only bonds between Zn atoms (pairs within rhomboid rings) are shown. Equivalent views for sections of the α-Zn_4Sb_3 (c) and the α-Cd_4Sb_3 structure (d). Grey circles denote interstitial Zn and Cd atoms.

(35) Mayer, H. W.; Mikhail, I.; Schubert, K. *J. Less-Common Met.* **1978**, *59*, 43.
(36) Mozharivskyj, Y.; Janssen, Y.; Harringa, J. L.; Kracher, A.; Tsokol, A. O.; Miller, G. J. *Chem. Mater.* **2006**, *18*, 822.

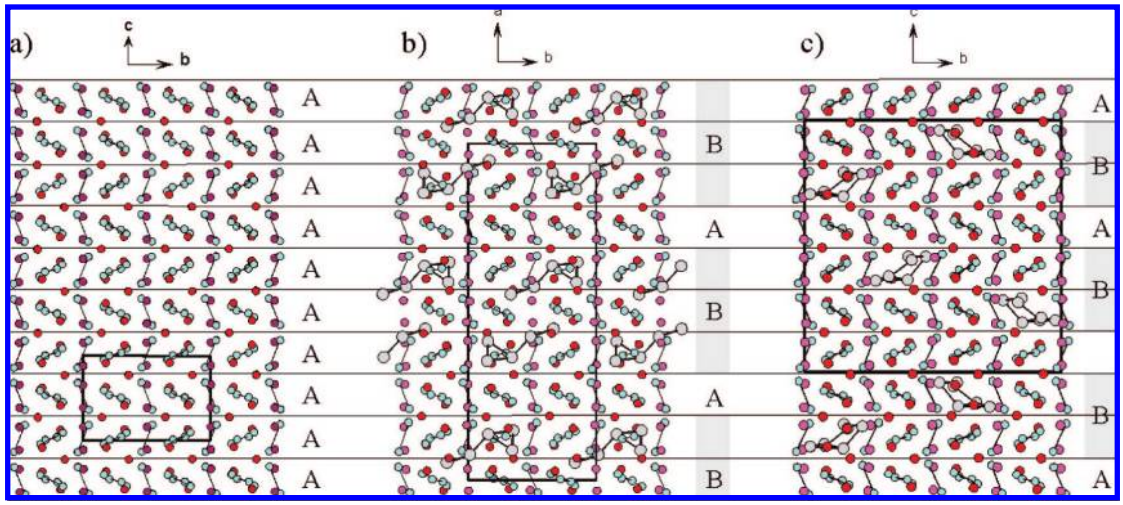

Figure 7. Comparison of the crystal structures of β-Zn_4Sb_3 (idealized, disorder-free framework $Zn_{12}Sb_{10}$) (a), α-Zn_4Sb_3 (b), and α-Cd_4Sb_3 (c). For the rhombohedral β-Zn_4Sb_3 structure a monoclinic unit cell is indicated. The color code is as in Figure 6. A denotes a lamellae building unit with a composition $Zn(Cd)_{12}Sb_{10}$. B denotes a block of lamellae hosting aggregates of interstitial atoms (and vacancies). Bonds are drawn between pairs of Zn(Cd) atoms being part of rhomboid rings (turquoise circles) and between interstitial divalent atoms (gray circles).

and α-Cd_4Sb_3 are four and six times larger, respectively, than the one of the disordered β-phase.

Next we have a closer look at the interstitial divalent metal atoms (Figure 8). The two Sb positions of the rhombohedral β-Zn_4Sb_3 framework split into 20 independent positions in the α-structure, while Zn occupies 26 independent positions. Twenty-one out of the 26 Zn positions in α-Zn_4Sb_3 correspond to regular framework Zn atoms arranged in pairs within the rhomboid rings in β-Zn_4Sb_3. As a matter of fact, there is a striking 1:1 correspondence. The remaining five positions are then associated with interstitial Zn atoms (which are randomly distributed in disordered β-Zn_4Sb_3. These atoms are assembled in clusters consisting of a triangle with a tail of two more Zn atoms (Figure 8a). Two five-atom clusters are grouped together and related by a center of inversion. Each pair of five-atom clusters replaces three pairs of Zn atoms from the regular rhomboid ring framework in β-Zn_4Sb_3. These missing pairs of Zn atoms are associated with vacancies (which are randomly distributed in β-Zn_4Sb_3).

A similar analysis for α-Cd_4Sb_3 leads to a different result. There are 60 and 78 independent Sb and Cd positions, respectively, in the unit cell. Now 64 out of the 78 Cd positions correspond to regular framework Cd atoms arranged in pairs, and the remaining 14 correspond to interstitials Cd atoms. These atoms aggregate into chains running along the *a*-direction of the structure (Figure 8b; cf. Figure 7c). One chain has 7 atoms in the repeat unit and replaces two pairs of Cd atoms from the regular framework (vacancies). The unit cell contains two symmetrically unrelated chains that, however, appear to be indistinguishable as a result of translational pseudo symmetry. This pseudo symmetry is incompatible with inversion symmetry between the two chains, and hence the two are truly independent. Figure 8c compares the arrangements of interstitial divalent metal atoms in α-Zn_4Sb_3 and α-Cd_4Sb_3. Both arrangements display a triangle of atoms as the central feature. In α-Zn_4Sb_3 they are part of confined clusters with a separation of at least 4.4 Å while in α-Cd_4Sb_3 they are part of an extended chain. Importantly, arrangements of interstitials always replace pairs of divalent atoms from rhomboid rings of the regular framework.

The fraction of interstitials among the divalent metal component in α-Zn_4Sb_3 and α-Cd_4Sb_3 as determined from crystallography is close to 20%. It is assumed that the ordered interstitials in the α-phases become randomly distributed in the β-phases which amounts to a substantial degree of disorder in the latter. The reversible order−disorder α-β transition is intriguing and its mechanism has not been revealed yet. In this respect Zn_4Sb_3 is actually more complicated than Cd_4Sb_3 because the Zn deficiency with respect to the ideal composition $Zn_{13}Sb_{10}$ triggers a further transition to α'-Zn_4Sb_3 at 235 K. The formation of α'-Zn_4Sb_3 corresponds to a further step of ordering, now with respect to the Zn deficiency. In the α'-Zn_4Sb_3 structure interstitial Zn atoms are arranged as in the α-Zn_4Sb_3 structure but the lamellae theme is modulated.[20] The twinning and the relatively complex superstructure of α-Cd_4Sb_3 makes detailed structural studies quite demanding. In particular, our diffraction data do not allow for any dependable refinement of occupancies for the ordered interstitials. In α-Zn_4Sb_3 high quality diffraction data revealed a remnant disorder by which the replacement of pairs of regular Zn positions by ordered interstitials is incomplete. This leads to a composition that is inherently Zn deficient, $Zn_{13-\delta}Sb_{10}$. While this is also noticeable in microprobe elemental analysis of Zn_4Sb_3 samples,[20] melt-quenched α-Cd_4Sb_3 indicates no such deficiency (cf. Table 2).

Physical Properties of α-Cd4Sb3. What are the consequences of the peculiar structural properties of Cd_4Sb_3 for the physical properties? There are early reports on the electrical properties of Cd_4Sb_3 which, however, differ widely.[23] It has been suspected that these variations reflect uncertainties in the actual Cd−Sb phases measured. Further, Zelinska et al. reported the electrical resistivity of their Cd_4Sb_3 sample which had been characterized to possess the disordered β-Cd_4Sb_3 structure at room temperature. They found a magnitude of 7 mΩcm at room temperature, and to decrease as the temperature was lowered.[24]

Figure 9 compiles thermopower, resistivity and thermal conductivity of our samples which were measured between 10 and 350 K. The thermopower exhibits a positive temperature dependence and attains large values when approaching room temperature (Figure 9a). At 300 K the magnitudes for melt-quenched and Bi-flux sample are similar, 150 and 160 μV/K, respectively, while the one for the Sn-flux sample is considerably higher and exceeds 400 μV/K. For comparison, room temperature values for the thermopower of Zn_4Sb_3 have been reported

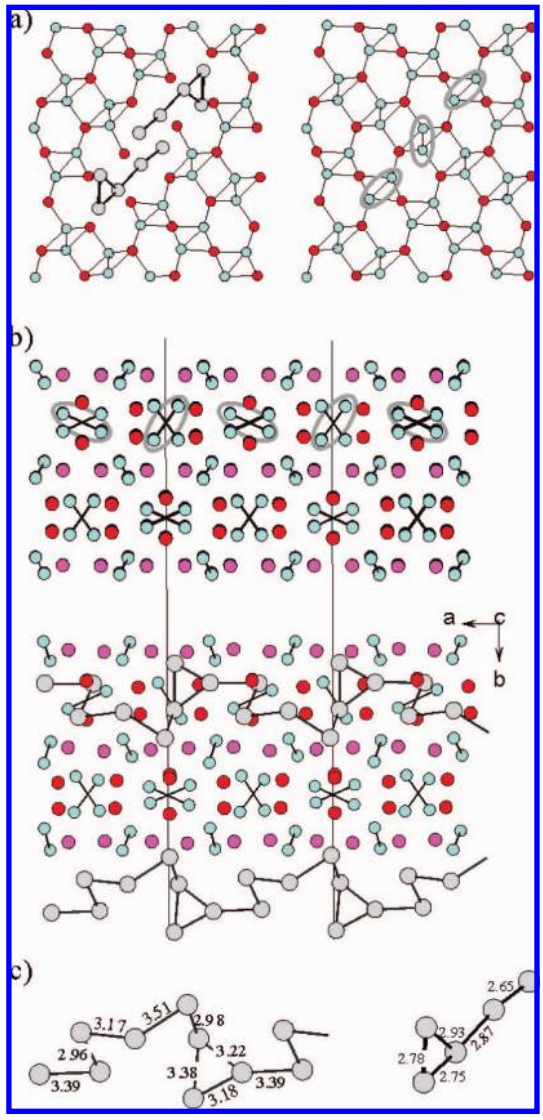

Figure 8. (a) Equivalent sections of the triclinic α-Zn_4Sb_3 structure (left) and the rhombohedral $Zn_{12}Sb_{10}$ framework idealizing β-Zn_4Sb_3 (right). Sb2 atoms are omitted for clarity. Regular ("rhombohedral") Zn atoms are drawn as turquoise and interstitial Zn atoms (arranged as five-atom clusters) as gray circles. In the section of the $Zn_{12}Sb_{10}$ framework the pairs of regular Zn atoms corresponding to vacancies in α-Zn_4Sb_3 are high-lighted. Two five-atom clusters of interstitials replace three pairs of Zn atoms from the rhombohedral framework. (b) Equivalent sections of the rhombohedral $Cd_{12}Sb_{10}$ framework idealizing β-Cd_4Sb_3 (top) and the monoclinic α-Cd_4Sb_3 structure (bottom). Interstitial Cd atoms (gray) are arranged in chains. The repetition unit is indicated by vertical lines. One chain of interstitials replaces two pairs of Cd atoms from the rhombohedral framework. (c) Comparison of the interstitials arrangements in α-Cd_4Sb_3 (left) and α-Zn_4Sb_3 (right). The inserted numbers are interatomic distances in Å.

between 70 and 160 μV/K, depending on sample preparation and doping. The thermopower of Cd_4Sb_3 displays a pronounced discontinuity where either the slope changes markedly (for melt-quenched and Bi-flux samples at around 150 and 250 K, respectively) or even a maximum occurs (for the Sn-flux sample, at around 300 K). The pronounced discontinuity for the Sn-flux sample may be connected with a structural change. We only performed low-temperature structural studies for the melt-quenched sample where single crystal X-ray diffraction data sets collected at 100 and 295 K refined to the same structure. Note that the temperature where the thermopower attains a

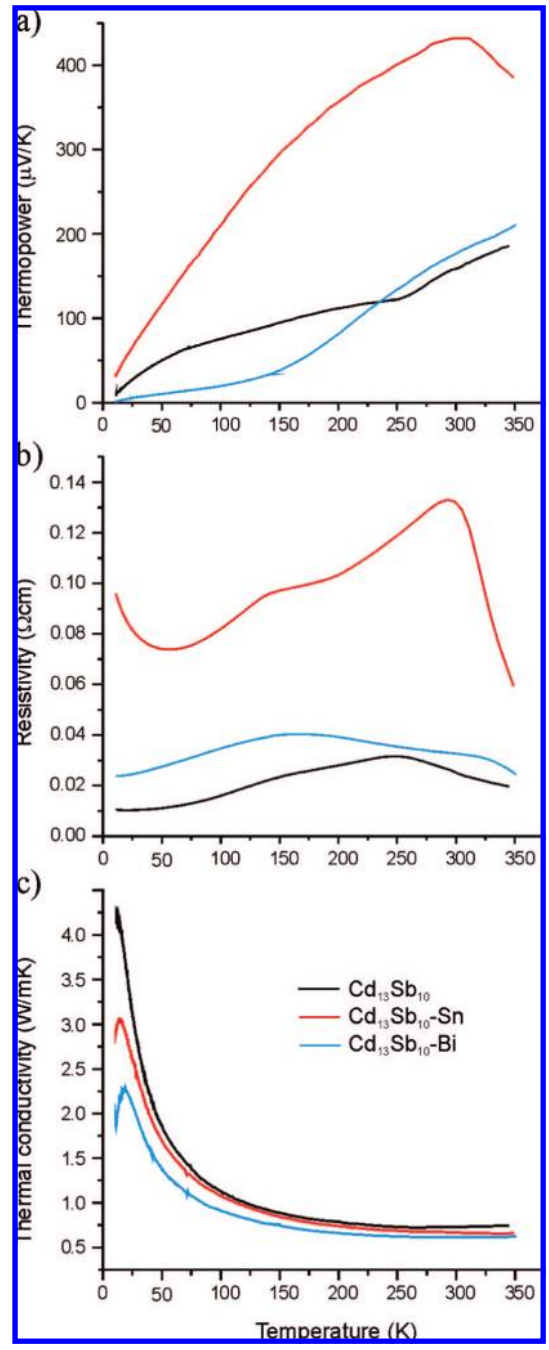

Figure 9. Thermopower (a), electrical resistivity (b), and thermal conductivity (c) of melt-quenched (black lines), Bi-flux (blue lines), and Sn-flux (red lines) prepared samples of Cd_4Sb_3.

maximum for the Sn-flux sample is below that of the α-β transition as established from DSC analysis (cf. Figure 5).

The resistivity of our Cd_4Sb_3 samples displays a complicated temperature dependence in the investigated temperature interval (Figure 9b). The positive sign of the Seebeck coefficient implies that holes are the majority charge carriers. At 75 K and higher temperatures the resistivity behavior is metallic-like, and changes at a certain temperature into a semiconductor-like one. The temperature where the resistivity attains a maximum coincides with the discontinuity in the thermopower (cf. Figure 9a). The room temperature resistivity for the melt-quenched and Bi-flux sample is 0.026 and 0.033 Ωcm, respectively. This is an order of magnitude higher than reported room temperature resistivity

for Zn_4Sb_3 samples (1−3.5 mΩcm) and disadvantageous if considering Cd_4Sb_3 as a thermoelectric material. Zn_4Sb_3 is slightly Zn deficient with respect to the ideal composition $Zn_{13}Sb_{10}$ which, according to theoretical calculations, yields a narrow band gap of 0.3 eV and a fully occupied valence band for ordered α-Zn_4Sb_3.[37] It is plausible to assume that the Zn deficiency of Zn_4Sb_3 relates to a more metallic behavior and that a corresponding phenomenon is much less pronounced in Cd_4Sb_3.

Again, as for the thermopower, the resistivity of the Sn-flux sample is distinguished from the other samples. First, magnitudes are around 0.1 Ωcm and, thus, almost an order of magnitude larger. Second, it exhibits a peculiar minimum around 50 K where resistivity increases again with decreasing temperature. This feature is actually also present as a weak upturn in the other samples, but occurs at lower temperatures (around 35 K). We note that the temperature dependent resistivity of our samples differ profoundly from that reported by Zelinska et al.[24] This supports the possibility that these authors may have indeed obtained Cd_4Sb_3 with the disordered β-phase structure at room temperature. Interestingly, Zelinska et al. reported also a shallow upturn of the resistivity near 35 K for their sample. The resistivity behavior of α-Cd_4Sb_3 may be interpreted as follows. The phase represents a degenerate narrow gap semiconductor with a very low concentration of native impurities. Therefore the resistivity decreases with increasing temperature already at the lowest temperatures due to an increase in the charge carrier concentration. Above some temperature (near 35 and 50 K) the expected further decrease of resistivity is balanced by a decreasing mobility of carriers probably associated with the increased thermal motion of loosely bonded interstitial Cd atoms, acting as impurity scatterers. At high temperatures this phenomenon exhausts and is balanced by the further increased carrier concentration, after which the resistivity takes again a semiconductor-like behavior. The proof of this hypothesis would require measurements of the temperature dependency of carrier concentration and mobility. This includes especially the Sn-flux sample which appears to be distinguished from the others. We note that metal doping has also large consequences to the structural and thermoelectric properties of Zn_4Sb_3 but is not well understood.[20,38]

Finally we discuss the thermal conductivity (Figure 9c) which is similar for the different Cd_4Sb_3 samples. From the measured value of the resistivity and the Wiedemann−Franz law, the electronic contribution to the thermal conductivity is estimated to be less than 5%. Thus, the measured thermal conductivity is essentially the lattice thermal conductivity. The very steep rise with decreasing temperature is characteristic of predominant phonon−phonon Umklapp scattering, which can be observed in well crystalline and compositionally pure samples.[10,39] Umklapp scattering has a 1/T dependency above Θ_D, the Debye temperature, and indeed the data for our samples decay in a $1/T$ manner for the temperature range 50−290 K. The sharp upturn of the thermal lattice conductivity at lower temperatures—where the probability of Umklapp scattering is small—has usually a $e^{\Theta D/2T}$ dependence. The maximum of the thermal conductivity is reached when the phonon mean free path becomes comparable to the crystal dimension. Above 130 K the thermal conductivity of our samples has dropped below 1 W/mK and room temperature values are in a range of 0.6 to 0.8 W/mK. This is comparable to the room temperature thermal lattice conductivity for β-Zn_4Sb_3 (0.65−1.15 W/mK). Across the low-temperature structural phase transitions (235−255 K) the thermal conductivity of Zn_4Sb_3 rises by about 15%.[19,21] Thus, the thermal lattice conductivity of ordered α- and α′-Zn_4Sb_3 is actually higher than that of α-Cd_4Sb_3.

The low lattice thermal conductivity of both, Zn_4Sb_3 and Cd_4Sb_3 is truly remarkable because the property is isotropic and inherent to crystalline, fully dense, binary compounds. According to Slack, the probability of Umklapp scattering scales linearly with the lattice parameter[9] and a simple explanation for the low thermal lattice conductivity of these systems would be their large unit cell crystal structures. However, the generalized formula derived by Slack for the calculation of thermal lattice conductivity is based on a simple Debye phonon distribution. This cannot be necessarily expected for the low-temperature modifications of Cd_4Sb_3 and Zn_4Sb_3—where clusters or chains of interstitials may be more loosely bonded than atoms constituting the rhomboid ring framework—and more complex phonon scattering mechanisms are likely.

Conclusions

The metastable intermetallic compound Cd_4Sb_3 was synthesized and structurally characterized. Cd_4Sb_3 has the crystallographic composition $Cd_{13}Sb_{10}$ ($Cd_{3.9}Sb_3$) and features a complex monoclinic structure with 276 atoms in the unit cell. The room temperature structure of Cd_4Sb_3 is similar to α-Zn_4Sb_3 which is a low-temperature modification of disordered, thermoelectric β-Zn_4Sb_3. Cd_4Sb_3 displays a reversible order−disorder transition at 373 K and decomposes into a stable mixture of elemental Cd and CdSb at around 520 K. Metal fluxes allow the preparation of large crystals of metastable Cd_4Sb_3 which are well suited for detailed structure and property characterization of this material. Cd_4Sb_3 combines semiconductor electron transport properties with a very low thermal conductivity. The behavior of the temperature-dependent resistivity is complicated and resistivity values are considerably higher than that for Zn_4Sb_3. The largely altered electronic properties observed in Sn-flux prepared Cd_4Sb_3 raise the expectation that it might be possible to dope Cd_4Sb_3 into a thermoelectric material superior to Zn_4Sb_3. However, the combination of low thermal stability and toxicity of Cd will hamper its use in practical applications.

Acknowledgment. This work was supported by the Swedish Research Council (V.R.) and NSF through Grants CHE-0612553 and DMR-0638826. We are grateful to Dr. Gordon Moore, ASU, for assistance with the microprobe analysis.

Supporting Information Available: Crystallographic information files for α-Cd_4Sb_3. This material is available free of charge via the Internet at http://pubs.acs.org.

JA805454P

(37) Mikhaylushkin, A. S.; Nylén, J.; Haussermann, U. *Chem.−Eur. J.* **2005**, *17*, 4912.
(38) (a) Tsutsui, M.; Zhang, L. T.; Ito, K.; Yamaguchi, M. *Intermetallics* **2004**, *12*, 809. (b) Liu, F.; Qin, X. Y.; Li, D. *J. Phys. D: Appl. Phys.* **2007**, *40*, 4974. (c) Pedersen, B. L.; Birkedal, H.; Nishibori, E.; Bentien, A.; Sakata, M.; Nygren, M.; Frederiksen, P. T.; Iversen, B. B. *Chem. Mater.* **2007**, *19*, 6304. (d) Litvinchuk, A. P.; Nylén, J.; Lorenz, B.; Guloy, A. M.; Häussermann, U. *J. Appl. Phys.* **2008**, *103*, 123524.
(39) Morelli, D. T.; Caillat, T.; Fleurial, J.-P.; Borshchevsky, A.; Vandersande, J.; Chen, B.; Uher, C. *Phys. Rev. B* **1995**, *51*, 9622.